Cureus Journal of Engineering

Open Access Original Article

Assessing the Corrosion Behaviour of Reinforcement Mild Steel in Simulated Coastal Marine Conditions of Walvis Bay, Namibia

Received 06/29/2025
Review began 07/04/2025
Review ended 10/10/2025
Published 10/28/2025

DOI:
https://doi.org/10.7759/s44388-025-07926-y

Silas I. Hango [1] , Melvin M. Mashingaidze [1] , Thomas S. Alweendo [1] , Nathan Kashweka [2]

1. Department of Mechanical and Metallurgical Engineering, University of Namibia, Ongwediva, NAM 2. Engineering, Namibian Ports Authority, Walvis Bay, NAM

Corresponding author: Silas I. Hango, shango@unam.na

Abstract

The coastal atmosphere of Walvis Bay, Namibia, is among the most corrosive in southern Africa due to persistent marine aerosols, high humidity, and temperature fluctuations. This study investigates the corrosion behaviour of reinforcement mild steel bars (rebars) under simulated marine conditions, using natural seawater and corrosion parameters derived from environmental data of the study area. Unlike conventional studies, this work integrates region-specific exposure data to realistically reproduce the aggressive marine conditions typical of splash and tidal zones. After 60 days of immersion, smaller diameter bars exhibited approximately 64.8% higher mass loss (0.095 ± 0.026 g) than larger bars (0.037 ± 0.001 g), corresponding to corrosion rates of 0.153 ± 0.021 mm/y and 0.076 ± 0.033 mm/y, respectively. SEM and XRD analyses revealed ferrite-pearlite microstructures and corrosion products such as Fe_2O_3, Fe_3O_4, γ-FeOOH, and α-FeOOH, confirming both uniform and localised corrosion. The results are the first publicly disseminated quantitative corrosion dataset for steel rebars in the Walvis Bay marine environment. The use of protective coatings, optimised concrete cover thickness, and periodic maintenance to mitigate steel degradation are highly recommended for reinforced structures in that area. These findings are useful for designing durable coastal infrastructure in Namibia and comparable marine environments. However, there is need for further detailed monitoring of environmental conditions to better understand their influence on the corrosion of exposed steel infrastructures at the coast of Walvis Bay.

Categories: Materials Engineering, Structural Engineering, Environmental and Sustainable Engineering
Keywords: corrosion, reinforcement steel, seawater, coastal environmental conditions, chlorine-induced corrosion, mass loss, corrosion rate, protective oxide layer, surface characterisation, iron oxide

Introduction

Corrosion poses a major challenge to steel infrastructures along the coast of Walvis Bay, Namibia. Key components such as steel rebars, vessel chains, wheel rim lock rings, railway track components, and buoys are highly susceptible to degradation, which weakens their mechanical properties and may lead to structural failure [1]. Corrosion of reinforcing mild steel is an electrochemical process that produces a complex mixture of oxides and oxyhydroxides such as Fe_2O_3, Fe_3O_4, α-FeOOH, γ-FeOOH, and $FeCl_2$, among others [2-8]. These corrosion products are generally porous and poorly adherent, allowing continued exposure of the metal surface to aggressive agents.

Mild steel is widely used in marine environments for its mechanical strength and cost-effectiveness [9-11]. However, it becomes highly prone to corrosion during long-term seawater exposure [12]. Researchers conducted in various coastal regions including Durban, Cape Town, Port Elizabeth, and Walvis Bay have shown that it exhibits some of the highest corrosion rates globally, ranging between 0.10 and 0.80 mm/year. These extreme rates are caused by the warm Benguela Current, frequent mist banks, reduced rainfall, and high onshore humidity [13,14]. The combined effects of oxygen, moisture, chloride, and sulphate ions further accelerate corrosion in intertidal and splash zones [15-19].

Temperature and relative humidity also play critical roles, as they promote electrochemical activity, fog formation, and deposition of marine aerosols [1,11,16,18,20-23]. Fog is particularly common along the Walvis Bay coast, where warm, moist air from the landmass condenses over cold coastal waters, creating highly corrosive atmospheric conditions [16,23].

Numerous studies have examined reinforcement steel corrosion in marine environments using electrochemical and immersion techniques [12,15,22-28]. Thus, immersion testing remains a reliable method for quantifying long-term corrosion performance by measuring mass loss and analysing the corrosion products through techniques such as scanning electron microscope (SEM) and X-ray diffraction (XRD).

How to cite this article
Hango S I, Mashingaidze M M, Alweendo T S, et al. (October 28, 2025) Assessing the Corrosion Behaviour of Reinforcement Mild Steel in Simulated Coastal Marine Conditions of Walvis Bay, Namibia. Cureus J Eng 2 : es44388-025-07926-y. DOI https://doi.org/10.7759/s44388-025-07926-y

This study evaluated the corrosion behaviour of mild steel rebars of different diameters in simulated Walvis Bay marine conditions, using immersion testing supported by SEM, XRD, and mass loss measurements. The novelty of this research lies in its focus on the unique marine microclimate of Walvis Bay, characterised by persistent fog, chloride-rich aerosols, and fluctuating humidity-factors rarely studied in combination. By integrating environmental data with laboratory immersion testing, the work provides site-specific insights into steel degradation and supports the development of corrosion protection strategies for coastal infrastructure in Namibia and similar environments.

Materials And Methods

Coastal marine conditions of Walvis Bay

The laboratory immersion tests were designed to reflect the corrosive marine environment of Walvis Bay using pre-collected environmental data. Ambient temperature and relative humidity data were sourced from the Namibia Meteorological Services, while seawater composition was analysed in the laboratory.

Temperature was set within the local range (25-45°C) due to its direct influence on corrosion kinetics. Natural seawater was used to maintain authentic chloride content, a key factor in steel degradation. While relative humidity does not affect submerged steel directly, the consistently high humidity in Walvis Bay supports the use of continuous immersion, simulating the always-wet conditions found in splash and tidal zones. This alignment of test conditions with local coastal parameters ensured the relevance and accuracy of the immersion corrosion simulations. The dataset spans four consecutive years and systematically analysed to identify temporal patterns and spatial variations that may affect marine corrosion mechanisms.

Characterisation of natural seawater

The seawater samples used for immersion testing were collected from Berth #3 at Walvis Bay, Namibia. The physicochemical parameters of the seawater were determined prior to the corrosion experiments in order to characterise the exposure medium. Measurements of pH, electrical conductivity (EC), redox potential (ORP), turbidity, and total dissolved solids (TDS) were performed using a calibrated multi-parameter probe (Hanna Instruments HI9829). Total hardness, Ca-hardness, and Mg-hardness were determined by complexometric titration with EDTA in accordance with APHA Standard Method 2340C [29].

Major anions such as chloride (Cl^-), fluoride (F^-), sulphate (SO_4^{2-}), nitrate (NO_3^-), and nitrite (NO_2^-) were quantified using ion chromatography (Metrohm 883 Basic IC Plus), while major cations such as sodium (Na), potassium (K), magnesium (Mg), and calcium (Ca) were analysed by inductively coupled plasma-optical emission spectroscopy (Agilent 5110). Trace and heavy metals, including manganese (Mn), iron (Fe), chromium (Cr), cadmium (Cd), lead (Pb), arsenic (As), and selenium (Se), were determined using inductively coupled plasma-mass spectrometry (Agilent 7900) for high sensitivity and precision.

The Langelier and Ryznar stability indices were calculated based on the measured pH, alkalinity, hardness, TDS, and temperature to assess the scaling or corrosive tendency of the seawater [16].

Characterisation of the rebars

The microstructural features of the reinforcement steel bars were examined using a Zeiss Gemini SEM 300 SEM to assess surface morphology and microstructural integrity. Phase analysis was conducted using XRD on a BRUKER® D8 ADVANCE diffractometer equipped with a Cu Kα radiation source (λ = 1.5406 Å). XRD scans were performed over a 2θ range of 10° to 90° to identify the crystalline phases present in the steel bars.

Corrosion measurements

Immersion tests were conducted on reinforcement steel coupons of two diameters (ø = 10 mm and ø = 20 mm, each with 10 mm thickness), each prepared with a centrally drilled 0.05 mm hole for ease of attaching to suspension strings. The chemical composition of the steel is provided in Table *1*. Prior to testing, the specimens were ground to 800 grit, ultrasonically cleaned in acetone, and rinsed with deionised water.

Filtered natural seawater, collected from Berth #3 in Walvis Bay, was used as the corrosive medium, with suspended particles and biological matter removed while retaining the chemical composition representative of local seawater. Full immersion testing was employed as a controlled approximation of the humid marine atmosphere, providing exposure representative of the coastal environment. Samples were immersed in individual open beakers (1 L each) under laboratory ambient temperature (24.3 ± 1.2 °C) and humidity (51.2 ± 1.4 %), allowing natural aeration throughout the exposure period. No renewal of the seawater was performed during the 60-day immersion.

For each condition, tests were performed in duplicate (n = 2 independent specimens per diameter), and the average value was recorded. Mass loss measurements were conducted at 5-day intervals. After each interval, the samples were removed, and corrosion products were carefully removed using a surgical blade and soft brush. The cleaned specimens were rinsed with deionised water, then dried with forced air followed by oven drying, and finally weighed to quantify the mass loss.

Corrosion rate was determined using equation 1. This procedure enabled the assessment of corrosion kinetics over time under the simulated marine exposure conditions.

$$Corrosionrate(mm/y) = K\frac{\Delta m}{\rho \cdot t \cdot A} \quad (2)$$

where, K = constant (8.74×10^4, to convert units to mm/y), Δm = mass loss (g) due to corrosion, ρ = density of metal (g/cm^3), t = exposure time (h), and A = exposed surface area of the sample (cm^2).

Sample	Element (wt.%)							
	Fe	C	Mn	Si	S	P	Cu	Ni
Large rebar	Bal.	0.18 ± 0.02	0.70 ± 0.10	0.20 ± 0.00	0.01 ± 0.00	0.01 ± 0.00	0.24 ± 0.03	0.07 ± 0.01
Small rebar	Bal.	0.16 ± 0.02	0.70 ± 0.20	0.14 ± 0.03	0.01 ± 0.00	0.01 ± 0.00	0.10 ± 0.02	0.03 ± 0.00

TABLE 1: Optical emission spectrographic analysis (wt.%) of reinforcement steel bars

Corrosion product characterisation

For XRD analysis of the corrosion products, loose rust deposits were carefully scraped from the outer surfaces of the corroded rebars and ground into a fine powder to ensure homogeneity. The XRD measurement procedure followed the methodology described by Hango et al. [30]. To complement the phase analysis, macrographs of the corroded steel surfaces were obtained using a Nikon COOLPIX L310 digital camera, providing visual documentation of the corrosion surface morphology and extent of degradation.

Results And Discussion

Pre-collected environmental data at the coast of Walvis Bay

Temperature

Hourly, daily, and monthly temperature variations were recorded over four years (1 January 2020-31 December 2023) (Figure *1*), to analyse their impact on the corrosion rates of mild steel rebars. The average annual temperature ranged between 14.8 °C and 23.6 °C, with daily maximums reaching up to 43.2 °C during summer and minimums dropping to around 10 °C in winter. The maximum temperature profiles exhibited consistent diurnal trends across all four years, with stable temperatures from 01:00 to 08:00, followed by a gradual rise between 09:00 and 15:00, peaking in the afternoon before declining between 16:00 and 20:00.

These daily maximum temperature cycles directly influence wet-dry alternations on exposed metallic surfaces, which accelerate the initiation and propagation of corrosion. This cyclical pattern is influenced by the strength of sea breezes in response to the land-sea temperature gradient, which promotes the penetration of corrosive ions onto exposed structures during temperature decreases around sunrise and sunset [22].

The diurnal temperature variability, with pronounced peaks during midday and lows in the early morning (Figure *2*), can be attributed to the inflow of fog and sea breezes, which is a common phenomenon at Walvis Bay [22]. These thermal fluctuations govern the time-of-wetness on metallic surfaces, a key parameter influencing corrosion rates [16,18,20]. The findings suggest that lower temperatures, particularly in July, may reduce corrosion, whereas elevated temperatures during typically cooler months could exacerbate material degradation in coastal environments [16,22]. This underscores the need for detailed monitoring of environmental conditions to better understand their influence on the corrosion of exposed steel infrastructures at the coast of Walvis Bay.

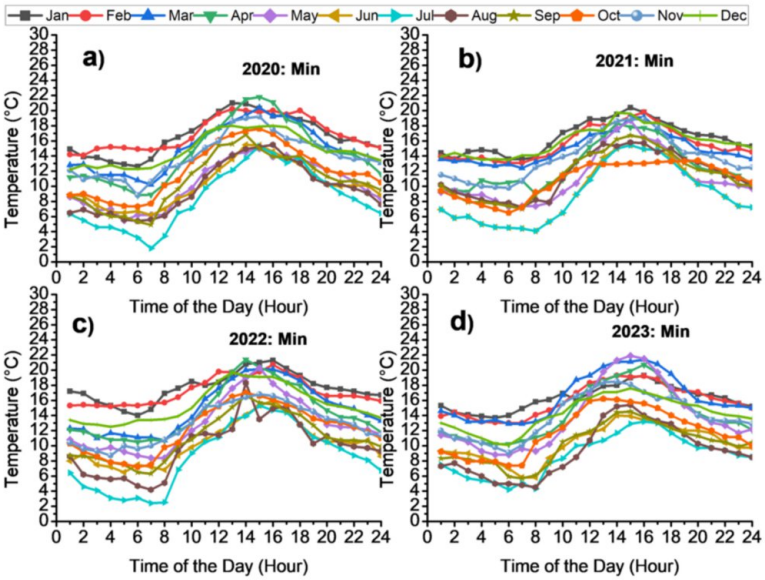

FIGURE 1: Daily variation of minimum temperatures at the coast of Walvis Bay, Namibia, in: (a) 2020, (b) 2021, (c) 2022, and (d) 2023

Humidity

The hourly, daily, and monthly humidity variations (Figure *3*) from 2020 to 2023 show clear diurnal and seasonal patterns that contribute significantly to the corrosion processes at the coast of Walvis Bay, Namibia. Relative humidity (RH) ranged from 55% to 95%, with an annual mean of ~78 ± 4%. Early-morning and night-time RH peaked at 85-95%, while daytime lows fell to 50-60% RH.

The high humidity during morning and night is primarily due to sea fog carrying marine aerosols such as Cl^-, Na^+, Mg^{2+}, SO_4^{2-}, NO_3^-, and SO_2 [31], which condense on steel surfaces, leading to the breakdown of protective layers, localised pitting, and general corrosion.

Minimum RH trends (Figure *4*) mirrored maximum values, with occasional drops below 45% RH between April and July, and irregular variations in August, reflecting seasonal transitions.

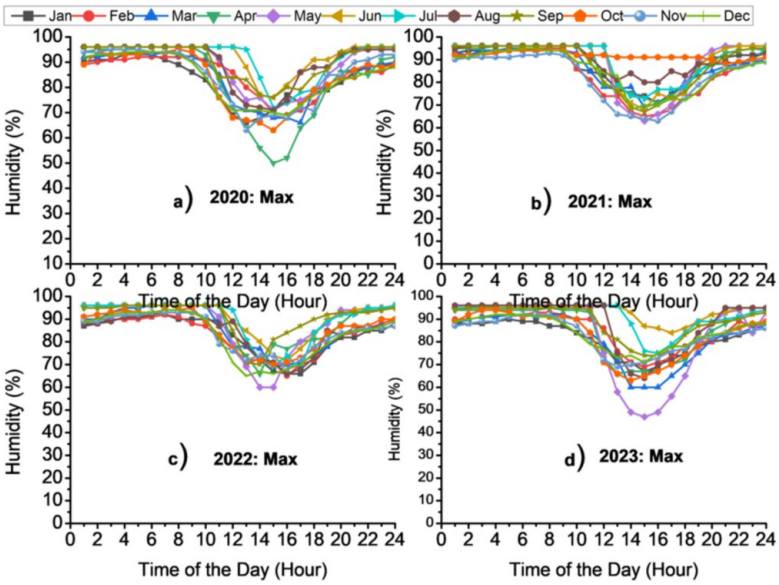

FIGURE 2: Daily variation of maximum humidity (%) at the coast of Walvis Bay, Namibia, in: (a) 2020, (b) 2021, (c) 2022, and (d) 2023

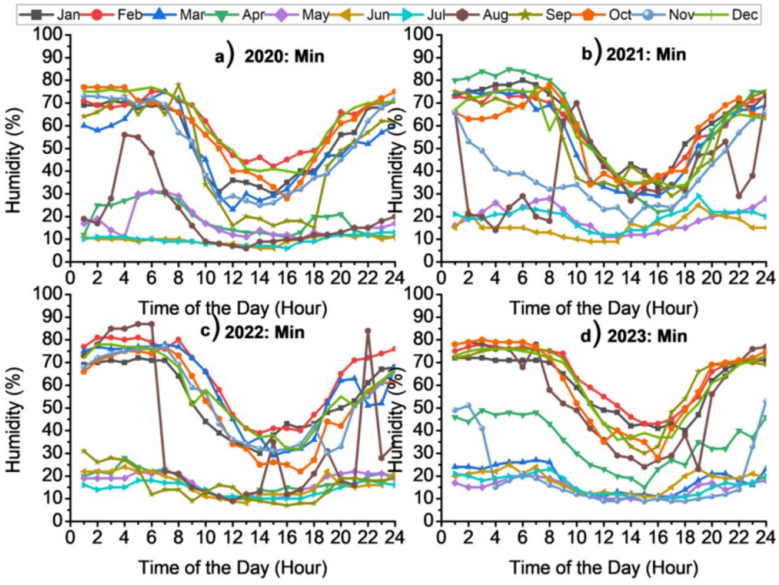

FIGURE 3: Daily variation of minimum humidity (%) at the coast of Walvis Bay, Namibia, in: (a) 2020, (b) 2021, (c) 2022, and (d) 2023

Analyses of natural seawater at Walvis Bay

The results of the seawater analysis are given in Table *2*. The water samples exhibited consistent physicochemical properties characteristic of open, non-restricted marine environments. These results confirmed the inherently corrosive nature of the Walvis Bay marine environment and its significant impact on steel infrastructure.

Parameter	Berth #3	Typical seawater	Eastern Mediterranean seawater	Arabian Gulf at Kuwait	Red Sea at Jeddah	Typical ocean water	Units
pH	7.3	-	-		-	-	-
Conductivity	5620	-	-		-	-	$mS{\cdot}m^{-1}$
Potential	194	-	-		-	-	mV
Turbidity	1.3	-	-		-	-	NTU
Hardness	6945	-	-		-	-	$mg{\cdot}L^{-1}$
NO_3^-	0.5	-	-		-	-	$mg{\cdot}L^{-1}$
Langelier Index	0.4	-	-		-	-	-
Ryznar Index	6.6						
Cl^-	22830.0	18980.0	21200.0	23000.0	22219.0	19353.0	$mg{\cdot}L^{-1}$
F^-	0.8	1.0	-	-			$mg{\cdot}L^{-1}$
SO_4^{2-}	3141.0	2649.0	2950.0	3200.0	3078.0	2712.0	$mg{\cdot}L^{-1}$
Na^+	12080.0	10556.0	11800.0	15850.0	14255	10781.0	$mg{\cdot}L^{-1}$
K^+	437.0	380.0	463.0	460.0	210.00	400.0	$mg{\cdot}L^{-1}$
Mg^{2+}	1410.0	1262.0	1403.0	1765.0	7420.0	1284.0	$mg{\cdot}L^{-1}$
Ca^{2+}	456.0	400.0	423.0	500.0	225.0	412.0	$mg{\cdot}L^{-1}$
Sr^{2+}	N/M	13.0	-	-		8.0	$mg{\cdot}L^{-1}$
HCO_3^-	N/M	140.0	-	142.0	146.0	126.0	$mg{\cdot}L^{-1}$
Br^-	N/M	65.0	155.0	80.0	72.0	844.0	$mg{\cdot}L^{-1}$
TDS	36963.0	-	34483.0	38600.0	45000.0	-	$mg{\cdot}L^{-1}$

TABLE 2: Chemical analysis of Walvis Bay natural seawater (Berth #3) and its comparison with other seawaters

pH

The pH of the seawater at Berth #3 was measured at 7.3 (Table *2*), slightly below the typical marine range of 7.5-8.2 [27]. Although still alkaline, this lower-than-expected value suggests increased CO_2 absorption and higher dissolved carbonate content, which may lower buffering capacity and destabilise passive oxide films on steel surfaces [32]. Hence, the mildly aggressive pH, combined with other environmental factors, likely contributes to the deterioration of steel infrastructure in the area.

Electrical conductivity and redox potential

The electrical conductivity of the seawater at Berth #3 was recorded at 5620 $mS{\cdot}m^{-1}$, exceeding values reported for regions like the Southern Baltic Sea and the South Pacific Ocean [26,27]. This elevated conductivity reflects high concentrations of dissolved salts, particularly Cl^-, SO_4^{2-}, and CO_3^{2-}, indicating the ability of the seawater to transport corrosive species [28]. In such saline environments, these anions can penetrate protective coatings or concrete pores, accelerating steel corrosion. Additionally, the redox potential of 194 mV was notably lower than the typical seawater value of ~250 mV [33], indicating reduced oxidising strength likely due to lower dissolved oxygen or localised stagnation [16]. Despite this, the positive redox value still supports electrochemical corrosion by facilitating metal oxidation.

Total dissolved solids and hardness

The TDS levels of 6945 mg·L^{-1} confirm the classification of Walvis Bay seawater as highly saline [26], promoting strong electrolytic behaviour and material degradation [27]. High salinity correlates with greater ion mobility and aggressive corrosion mechanisms [16,26]. In contrast, hardness-measured as 5806 mg·L^{-1} for Mg and 1139 mg·L^{-1} for Ca (as $CaCO_3$)-was significantly higher than comparable marine zones like Ujung Kulon Beach, Indonesia [34]. Although such hardness can foster scale formation that inhibits corrosion, the overwhelming presence of aggressive anions (Cl^-, SO_4^{2-}) and high TDS likely undermine this protective effect [16].

Ionic composition and stability indices

The seawater revealed exceptionally high levels of Cl^- (22830 mg·L^{-1}), SO_4^{2-} (3141 mg·L^{-1}), and alkali/alkaline earth metals such as Na^+ (12080 mg·L^{-1}), K^+ (4370 mg·L^{-1}), Mg^{2+} (1410 mg·L^{-1}), and Ca^{2+} (456 mg·L^{-1}) (Table *2*). These ions disrupt protective oxide layers and enhance localised corrosion processes, especially pitting [19]. Even trace levels of F^- and NO_3^- can act synergistically to increase corrosion rates [35,36], particularly in reinforced concrete systems [37]. The Langelier Index (LI = 0.4) indicates a tendency towards scale formation, while the Ryznar Index (RI = 6.6) suggests a marginally stable system (6.5-7.5). However, the corrosive influence of Cl^- and SO_4^{2-} overrides the scale-forming potential, creating a complex chemical environment where corrosion is more dominant than protection [16].

Comparison of the Walvis Bay seawater with other seawaters

To contextualise the ionic profile of the Walvis Bay seawater, samples from Berth #3 were benchmarked against two standard seawater compositions, and seawater analyses of three regional bodies with prominence in the maritime industry and trade-the Eastern Mediterranean Sea, Arabian Gulf, and Red Sea [38]. This comparative analysis serves both to validate the present findings and to support the future seawater analogues for remote corrosion studies.

Despite geographical variability, the Walvis Bay seawater exhibited an ionic hierarchy typical of marine systems: $Cl^- > Na^+ > SO_4^{2-} > Mg^{2+} > Ca^{2+} > K^+ > HCO_3^- > Br^- > BO_3^- > Sr^{2+} > F^- > H^+$. This similarity reinforces the reliability of the collected data and suggests that Walvis Bay shares the corrosive characteristics observed in other high-salinity environments. The dominance of chloride and sulphate ions, both of which aggressively compromise passive films on steel, highlights the significant threat of the marine environment to structural integrity. These findings support the broader corrosion assessment that the seawater at this coastal area is highly corrosive, and that the Walvis Bay marine environment is chemically comparable to other well-documented corrosive seawater systems.

Microstructure and XRD measurements before immersion tests

The SEM analysis of both large and small rebars (Figure *5a* and b) revealed a typical ferrite-pearlite microstructure, characteristic of mild steels [39]. Ferrite (α-Fe), the soft and ductile phase with a body-centered cubic structure, provides good toughness and formability but offers limited corrosion resistance due to its high iron content and low alloying [40]. Pearlite, a lamellar mixture of ferrite and cementite (Fe_3C), contributes to strength and hardness, though its electrochemical heterogeneity promotes micro-galvanic corrosion, with cementite acting as a cathode [41].

The XRD patterns of the samples (Figure *5c*) are identical, and confirm the presence of α-Fe and Fe3C phases in both bars. The relative intensity of pearlite features may suggest slight compositional or cooling rate differences, but both rebar samples conform to typical reinforcement steel standards [39]. The predominance of ferrite suggests good ductility, which is a trait of mild steels, while the cementite improves strength and hardness but compromises uniform corrosion resistance [39,40,42], especially in chloride-rich marine environments like Walvis Bay.

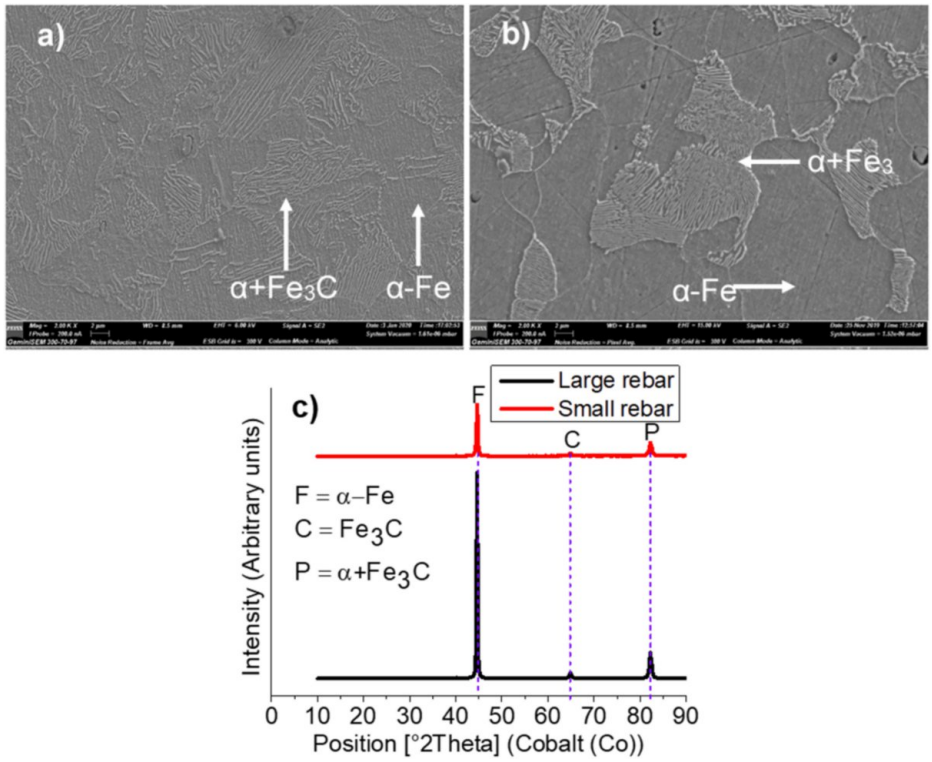

FIGURE 4: SEM micrographs of: (a) large reinforcement steel bar, and (b) small reinforcement steel bar, both revealing a typical ferrite–pearlite microstructure. The corresponding XRD patterns (c) confirm the presence of α-Fe and α-Fe + Fe_3C (cementite) phases

SEM, scanning electron microscope; XRD, X-ray diffraction

Immersion measurements

Mass Loss Analysis

Figure *6a* shows the progression of mass loss over a 60-day period for both bar sizes, which were immersed separately in natural seawater samples from Walvis Bay. Mass loss increased almost linearly during the first 40 days for both rebar samples. Thereafter, a slight plateauing was observed for the large bar after 60 days while the mass loss increased significantly for the small bar in the same time interval.

These results show a clear trend of progressive deterioration, with the small bar experiencing approximately 64.82% higher cumulative average mass loss (0.095 ± 0.026 g) than the large bars (0.037 ± 0.001 g) by Day 60. This behaviour is attributed to the higher surface-area-to-volume ratio of the smaller bars, which enhances exposure to chloride attack and oxygen diffusion [43]. Visual examination confirmed more corrosion products on the surface of the smaller bars, indicating severe localised corrosion than on larger bars [44]. The morphologies (Figure 7) provide intuitive insights into the formation of rust. It is evident that the rust layers exhibit different colours, attributed to the accumulation of corrosion products on the surface over prolonged exposure periods.

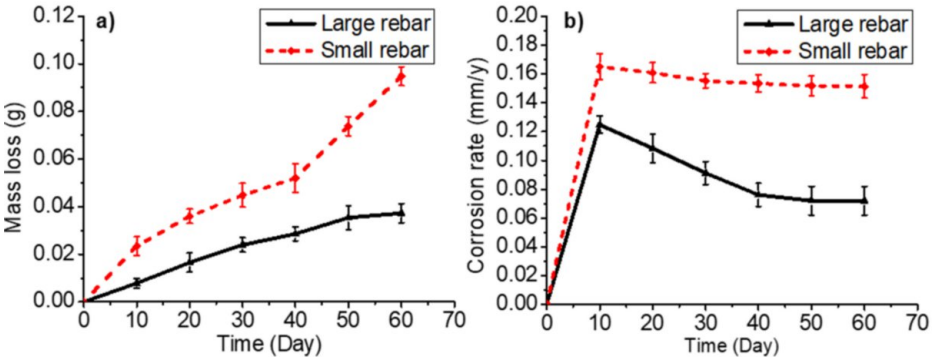

FIGURE 5: Variation of: (a) mass loss, and (b) corrosion rate with exposure time for the reinforcement steel bar samples immersed in the Walvis Bay natural seawater for 60 days

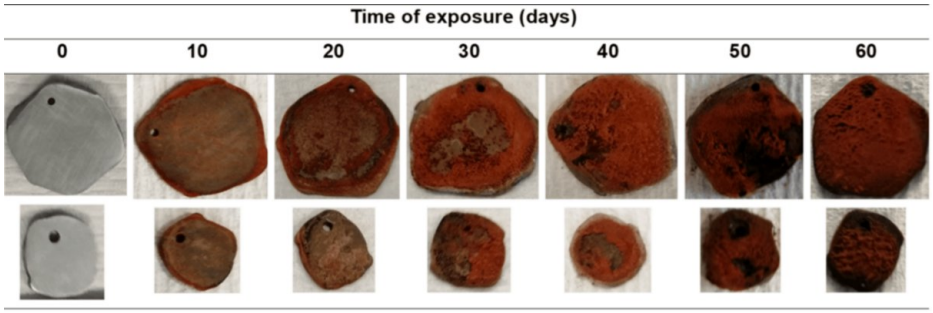

FIGURE 6: Macrograph of corroded large (upper) and small (lower) reinforcement steel bars from the coast of Walvis Bay after immersion test in natural seawater for the 60 days

Apart from geometric considerations, the higher mass loss observed in the small steel bars may also be microstructurally driven. The higher ferrite content in the smaller bars enhances their anodic behaviour in seawater, leading to intensified electrochemical dissolution when coupled with the more cathodic pearlite regions [43,44]. In contrast, the large bars, with greater pearlite content, show improved corrosion resistance due to more balanced microstructure and reduced micro-galvanic activity [45].

Corrosion Rate Analysis

Corrosion rates are presented in Figure *6b*. Both bar types showed a sharp decrease in corrosion rate between Day 10 and Day 40, indicative of aggressive electrochemical activity during the early immersion period. The peak corrosion rate for small bars reached 0.153 ± 0.021 mm/year at Day 30, while large bars exhibited a lower peak of 0.076 ± 0.033 mm/year over the same interval.

A subsequent decline in corrosion rates was observed between Day 40 and Day 60, possibly due to the formation of corrosion product layers acting as partial barriers to oxygen diffusion [40]. However, the rate reduction was more pronounced in the large bars, which retained comparatively intact oxide layers, suggesting enhanced passivity.

The high corrosion rate of the small rebars in seawater reflects the combined influence of their microstructural features, phase composition, and elemental makeup. A higher proportion of ferrite (α-Fe) in the small bars, compared to the larger ones, made them more susceptible to uniform corrosion, as ferrite acts as the anodic phase. In contrast, cementite (Fe_3C) within the pearlite regions behaves cathodically, promoting localised attack through micro-galvanic coupling [39,42]. This microstructural heterogeneity contributes significantly to the observed mass loss and surface degradation in the smaller bars.

XRD analysis confirmed the dominance of α-Fe and Fe_3C phases, typical of mild steel. The absence or minimal presence of corrosion-resistant alloying elements (e.g., Cr, Ni, or Cu) limits the ability of material to form a stable passive film in chloride-rich environments. Elemental analysis further revealed a high

iron content and low alloying additions, reinforcing the vulnerability of steel to chloride-induced corrosion in the aggressive marine atmosphere of Walvis Bay.

Corrosion Product Analysis

Phase evolution of corrosion products: The XRD patterns (Figure 7) revealed the presence of iron (Fe), hematite (Fe_2O_3), magnetite (Fe_3O_4), lepidocrocite (γ-FeOOH), and goethite (α-FeOOH) as dominant crystalline corrosion products, with varying intensities depending on the exposure duration and local surface morphology. The initial stages of immersion (10-40 days) favoured the formation of γ-FeOOH as the predominant phase [44,46]. This is consistent with prior reports which show that γ-FeOOH forms rapidly in oxygenated neutral to mildly alkaline chloride-containing environments, such as natural seawater, due to its metastable nature [45]. With continued immersion (40-60 days), α-FeOOH and Fe_3O_4 became increasingly dominant. Goethite is thermodynamically more stable than lepidocrocite and forms through a dehydration pathway, indicating progression towards a more mature corrosion product layer [42,44,46].

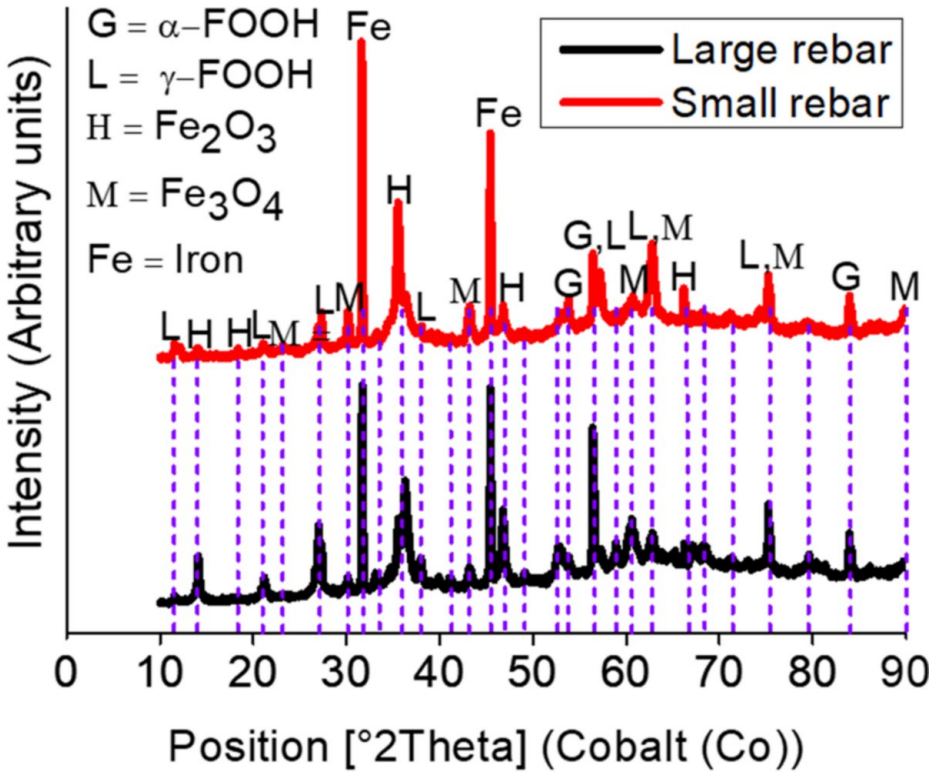

FIGURE 7: XRD pattern of the corrosion product layer formed on reinforcement steel bar samples after 60 days of immersion in natural seawater at Walvis Bay. The identified phases include iron (Fe), hematite (Fe2O3), magnetite (Fe3O4), lepidocrocite (γ-FeOOH), and goethite (α-FeOOH). The marked lines indicate the corresponding diffraction peaks for each phase

XRD, X-ray diffraction

Fe_3O_4, observed in both short-term and long-term exposure samples, likely formed under localised oxygen-depleted zones beneath loose rust layers. The occurrence of Fe_2O_3 (hematite), particularly in longer exposure samples (40-60 days), can be attributed to the oxidative transformation of magnetite in oxygen-rich zones [47].

Influence of Microstructure and Chemical Composition

The SEM revealed a ferrite-pearlite microstructure with localised banding. The corrosion preferentially initiated along the pearlitic regions due to galvanic coupling between ferrite (anodic) and cementite (cathodic) phases [48,49].

The steel bars, as per spectrometric analysis (Table *1*), contained 0.24 ± 0.03 wt.% Cu, 0.70 ± 0.20 wt.% Mn, 0.18 ± 0.02 wt.% C, 0.20 ± 0.00 wt.% Si, and trace amounts of S and P, which were relatively low, suggesting minimal intrinsic resistance to chloride-induced corrosion [50,51]. However, the presence of Mn and Si promotes initial passivation, but does not significantly inhibit long-term corrosion in chloride environments.

Correlation Between the Coastal Marine Conditions and Mass Loss of the Samples

The mass loss of the rebars correlated strongly with the aggressive marine environment of Walvis Bay. High seawater chloride levels (22830 ppm), elevated humidity (>80%), and temperatures of 25-45 °C promoted rapid electrochemical reactions, breaking down passive films and sustaining corrosion during immersion and wet-dry cycles influenced by tidal fluctuations. Maximum mass loss and corrosion rates occurred after prolonged exposure, reflecting cumulative chloride ingress and oxygen availability.

Corrosion rates (0.076-0.153 mm/y) were slightly lower than those reported for the Arabian Gulf (up to 0.25 mm/y) [52], and comparable to South African marine sites (0.10-0.18 mm/y) [16], indicating that while chloride-driven mechanisms are universal, local climate and aerosol composition strongly modulate corrosion kinetics in Walvis Bay.

Salt aerosols and dissolved oxygen induced localised, non-uniform corrosion, forming porous products such as γ-FeOOH and Fe_3O_4 (identified by XRD), particularly in regions exposed to fluctuating wet-dry conditions. These findings underscore the importance of site-specific environmental and microstructural factors in evaluating the durability of coastal steel infrastructure.

Conclusions

This study assessed the corrosion behaviour of reinforcement steel under simulated coastal marine conditions representative of Walvis Bay, Namibia, using immersion testing, SEM, and XRD analysis. The following conclusions were drawn:

1. Site-specific environmental data, including four years of temperature, relative humidity, and seawater composition, guided the laboratory setup, ensuring realistic simulation of local conditions. These factors collectively accelerated electrochemical reactions on the steel surface, resulting in significant material degradation.

2. SEM micrographs revealed ferrite-pearlite microstructures, confirmed by XRD analysis, which influenced the progression of corrosion.

3. XRD confirmed that the corrosion products formed on both rebars consisted predominantly of Fe2O3, Fe3O4, γ-FeOOH, and α-FeOOH, indicating both uniform and localised corrosion mechanisms under marine exposure.

4. Corrosion rate analysis showed that smaller rebars exhibited higher corrosion rates (0.153 ± 0.021 mm/y) than larger rebars (0.076 ± 0.033 mm/y), highlighting the impact of diameter and surface area on degradation.

By combining a four-year environmental dataset for Walvis Bay with a comparative analysis of small and large rebars, this work provides unique, site-specific insights into coastal corrosion. The findings underscore the importance of tailored corrosion management strategies for infrastructure in highly aggressive marine environments.

Despite the global availability of corrosion prevention methods, there is limited application of such strategies tailored to the specific conditions of the Walvis Bay coastline. To mitigate the risk of premature degradation of steel structures in this aggressive marine environment, the following recommendations are proposed:

1. Use galvanised and epoxy-coated reinforcement bars to provide dual-layer protection against chloride ingress and marine aerosol deposition.

2. Apply cathodic protection systems, either sacrificial or impressed current, particularly for large or critical infrastructure exposed to constant marine influence.

3. Use low-permeability, marine-grade concrete to reduce ionic transport and moisture ingress into the reinforcement zone.

4. Incorporate corrosion inhibitors, either as admixtures in concrete or applied externally near rebar zones, to delay initiation and propagation of corrosion.

5. Incorporate cyclic wet-dry or salt fog exposure tests to more accurately simulate the real humidity conditions of the coastal atmosphere.

Additional Information

Author Contributions

All authors have reviewed the final version to be published and agreed to be accountable for all aspects of the work.

Concept and design: Silas I. Hango, Melvin M. Mashingaidze, Thomas S. Alweendo, Nathan Kashweka

Acquisition, analysis, or interpretation of data: Silas I. Hango, Melvin M. Mashingaidze, Thomas S. Alweendo, Nathan Kashweka

Drafting of the manuscript: Silas I. Hango, Melvin M. Mashingaidze, Thomas S. Alweendo, Nathan Kashweka

Critical review of the manuscript for important intellectual content: Silas I. Hango, Melvin M. Mashingaidze, Thomas S. Alweendo, Nathan Kashweka

Supervision: Silas I. Hango, Nathan Kashweka

Disclosures

Human subjects: All authors have confirmed that this study did not involve human participants or tissue. **Animal subjects:** All authors have confirmed that this study did not involve animal subjects or tissue. **Conflicts of interest:** In compliance with the ICMJE uniform disclosure form, all authors declare the following: **Payment/services info:** All authors have declared that no financial support was received from any organization for the submitted work. **Financial relationships:** All authors have declared that they have no financial relationships at present or within the previous three years with any organizations that might have an interest in the submitted work. **Other relationships:** All authors have declared that there are no other relationships or activities that could appear to have influenced the submitted work.

Acknowledgements

The authors wish to acknowledge the support received from the University of Namibia and the Namibian Ports Authority, Walvis Bay and Namibia Meteorological Services for the meteorological data.

References

1. Xu Y, Huang Y, Cai F, Lu D, Wang X: Study on corrosion behavior and mechanism of AISI 4135 steel in marine environments based on field exposure experiment. Science of the Total Environment. 2022, 830:154864. 10.1016/j.scitotenv.2022.154864
2. Quraishi M, Nayak D, Kumar R, Kumar V: Corrosion of reinforced steel in concrete and its control: an overview. Journal of Steel Structures & Construction. 2017, 03:1-6. 10.4172/2472-0437.1000124
3. Dean SW, Delgadillo GHD, Bushman JB: Marine corrosion in tropical environments. ASTM International. 2000, 320. 10.1520/stp1399-eb
4. Nandi SK, Tewary NK, Saha JK, Ghosh SK: Microstructure, mechanical properties and corrosion performance of a few TMT rebars. Corrosion Engineering, Science and Technology: The International Journal of Corrosion Processes and Corrosion Control. 2016, 51:476-88. 10.1080/1478422x.2016.1141744
5. Song Y, Jiang G, Chen Y, Zhao P, Tian Y: Effects of chloride ions on corrosion of ductile iron and carbon steel in soil environments. Scientific Reports. 2017, 7:1-13. 10.1038/s41598-017-07245-1
6. Zitrou E, Nikolaou J, Tsakiridis P, Papadimitriou GD: Atmospheric corrosion of steel reinforcing bars produced by various manufacturing processes. Construction and Building Materials. 2007, 21:1161. 10.1016/j.conbuildmat.2006.06.004
7. Poursaee A: 2 - Corrosion of steel in concrete structures. Corrosion of Steel in Concrete Structures. 2016, 19-33.
8. Saha JK: Corrosion of Constructional Steels in Marine and Industrial Environment. Frontier Work in Atmospheric Corrosion. Springer, New Delhi; 2013. 10.1007/978-81-322-0720-7
9. Kainuma S, Yang M, Ishihara S, Kaneko A, Yamauchi T: Corrosion protection of steel members using an Al-Zn base sacrificial anode and fiber sheet in an atmospheric environment. Construction and Building Materials. 2019, 224:880-93. 10.1016/j.conbuildmat.2019.07.067
10. Wu D, Ding Y, Su J, Li ZX, Zhao B: Experimental investigation into corrosion effect on buckling and low-cycle fatigue performance of high-strength steel bars. Engineering Structures. 2024, 312:118230. 10.1016/j.engstruct.2024.118230
11. Zhang D, Fan Z, Yang H, Xiong J, Wang S, Wu Q: Comparative study of the corrosion behaviors of different steels in high performance concrete under marine environment. International Journal of Electrochemical

Science. 2022, 17:221267. 10.20964/2022.12.65
12. Wang Y, Wharton JA, Shenoi RA: Ultimate strength analysis of aged steel-plated structures exposed to marine corrosion damage: A review. Corrosion Science. 2014, 86:42-60. 10.1016/j.corsci.2014.04.043
13. Verhoef LGW: The Soiling and Cleaning of Building Facades. Taylor & Francis Group, Routledge; 2004.
14. Kämpf P, Chapman J: The Benguela current upwelling system. Upwelling Systems of the World. Springer, Cham; 2016. 251-314. 10.1007/978-3-319-42524-5_7
15. Shittu AA, Kara F Jain RK, Ibrahim TK: Design of a typical offshore transportation system for external corrosion. American Journal of Engineering Research. 2016, 5:112-28.
16. McEwan J: Corrosion Control in Southern Africa. Corrosion Institute of Southern Africa, Johannesburg; 2004.
17. Amlch L: Influence of corrosion of reinforcing bars on the bond between steel and concrete. Engineering, Materials Science. 1996, 138379717.
18. Ahmad S: Reinforcement corrosion in concrete structures, its monitoring and service life prediction--a review. Cement and Concrete Composites. 2003, 25:459-71. 10.1016/s0958-9465(02)00086-0
19. Ormellese M, Berra M, Bolzoni F, Pastore T: Corrosion inhibitors for chlorides induced corrosion in reinforced concrete structures. Cement and Concrete Research. 2006, 36:536-47. 10.1016/j.cemconres.2005.11.007
20. Ahlström J, Tidblad J, Sederholm B, Wadsö L: Influence of chloride and moisture content on steel rebar corrosion in concrete. Materials and Corrosion. 2016, 67:1049-58. 10.1002/maco.201508799
21. Ward AD, Trimble SW, Burckhard SR, Lyon JG: Environmental Hydrology, 3rd edn. Taylor & Francis, Florida, USA; 2015. 10.1201/b19120
22. Brimelow JC, vanHeerden J: Surface temperature and wind fields over the Skeleton Coast (Namibia) and adjacent interior during SAFARI-92. Journal of Geophysical Research: Atmospheres. 1996, 101:23767-3775. 10.1029/96jd01220
23. Alcántara J, de la Fuente D, Chico B, Simancas J, Díaz I, Morcillo M: Marine atmospheric corrosion of carbon steel: A review. Materials. 2017, 10:406. 10.3390/ma10040406
24. Karolina S, Rüdiger G, Christian S, Stefan W, Michael K: Mapping atmospheric corrosion in coastal regions: methods and results. Journal of Photonics for Energy. 2012, 2:022003. 10.1117/1.jpe.2.022003
25. Vashi RT, Patel RN: Corrosion study of metals in marine atmosphere. Asian Journal of Chemistry. 2010, 22:1225-230. 10.1155/2009/509216
26. Zakowski K, Narozny M, Szocinski M, Darowicki K: Influence of water salinity on corrosion risk—the case of the southern Baltic Sea coast. Environmental Monitoring and Assessment. 2014, 186:4871-879. 10.1007/s10661-014-3744-3
27. Boerlage SFE: Measuring salinity and TDS of seawater and brine for process and environmental monitoring—which one, when?. Desalination and Water Treatment. 2012, 42:222-30. 10.1080/19443994.2012.683191
28. Fondriest Environmental, Inc. Conductivity, salinity and total dissolved solids. (2014). Accessed: March 3, 2014: https://www.fondriest.com/environmental-measurements/parameters/water-quality/conductivity-salinity-tds/.
29. Braun-Howland EB, Lipps WC, Baxter TE: Standard methods for the examination of water and wastewater. American Public Health Association (APHA). 2023,
30. Hango SI, Cornish LA, Chown LH: Comparative analysis of corrosion resistance in Ni-, Cu- and Co-based alloys in synthetic mine water. Bulletin of Materials Science. 2025, 48:108. 10.1007/s12034-025-03458-7
31. Lee YN, Springston S, Jayne J, et al.: Chemical composition and sources of coastal marine aerosol particles during the 2008 VOCALS-REx campaign. Atmospheric Chemistry and Physics. 2014, 14:5057-72. 10.5194/acp-14-5057-2014
32. Hou X, Gao L, Cui Z, Yin J: Corrosion and Protection of Metal in the Seawater Desalination. IOP Conference Series: Earth and Environmental Science. 2018, 108:022037. 10.1088/1755-1315/108/2/022037
33. Cooper LHN: Oxidation-reduction potential in sea water. Journal of the Marine Biological Association of the United Kingdom. 1937, 22:167-76. 10.1017/S0025315400011929
34. Dan M, Okatrina H: Sea water characterization at Ujung Kulon coastal depth as raw water source for desalination and potential energy. E3S Web of Conferences. 2018, 31:02005. 10.1051/e3sconf/20183102005
35. Yang L, Xu Y, Zhu Y, Liu L, Wang X, Huang Y: Evaluation of interaction effect of sulfate and chloride ions on reinforcements in simulated marine environment using electrochemical methods. International Journal of Electrochemical Science. 2016, 11:6943-958. 10.20964/2016.08.51
36. Al-Tayyib AJ, Shamim Khan M: Effect of sulfate ions on the corrosion of rebars embedded in concrete. Cement and Concrete Composites. 1991, 13:123-27. 10.1016/0958-9465(91)90007-5
37. Singh DDN, Ghosh R, Singh BK: Fluoride induced corrosion of steel rebars in contact with alkaline solutions, cement slurry and concrete mortars. Corrosion Science. 2002, 44:1713-735. 10.1016/s0010-938x(01)00179-2
38. Lenntech. Composition of sea water. (1998). Accessed: accessed July 29, 2023: https://www.lenntech.com/composition-seawater.htm.
39. Gladshtein LI, Larionova NP, Belyaev BF: Effect of ferrite-pearlite microstructure on structural steel properties. Metallurgist. 2012, 56:579-90. 10.1007/s11015-012-9619-3
40. Yilmaz A, Ozkan C, Sietsma J, Gonzalez-Garcia Y: Properties of passive films formed on ferrite-martensite and ferrite-pearlite steel microstructures. Metals. 2021, 11:594. 10.3390/met11040594
41. Katiyar PK, Maurya R, Singh PK: Corrosion behavior of plain carbon steels under different heat treatment conditions in freely aerated 3.5% NaCl solution. International Journal of Sustainable Building Technology and Urban Development. 2022, 13:44-68. 10.22712/susb.20220005
42. Pusparizkita YM, Fardilah VA, Aslan C, Jamari J, Bayuseno AP: Understanding of low-carbon steel marine corrosion through simulation in artificial seawater. AIMS Materials Science. 2023, 10:499-516. 10.3934/matersci.2023028
43. Prayitno D, Irsyad M: Effect of ratio of surface area on the corrosion rate. SINERGI. 2018, 22:7. 10.22441/sinergi.2018.1.002
44. Refait P, Grolleau AM, Jeannin M, Rémazeilles C, Sabot R: Corrosion of carbon steel in marine environments: role of the corrosion product layer. Corrosion and Materials Degradation. 2020, 1:198-218. 10.3390/cmd1010010
45. Zuo-Jiang S, Tian Z, Jiang X, Yu H, Sun D: Investigation on galvanic corrosion behavior of Q235 in deep-sea water/sediments of the South China Sea via manned deep diving. Journal of Materials Research and

Technology. 2023, 26:8822-835. 10.1016/j.jmrt.2023.09.195
46. Seechurn Y, Surnam BYR, Wharton JA: Marine atmospheric corrosion of carbon steel in the tropical microclimate of Port Louis. Materials and Corrosion. 2022, 73:1474-489. 10.1002/maco.202112871
47. Wang G, Wu Q, Li XZ, Xu J, Xu Y, Shi WH, Wang SL: Microscopic analysis of steel corrosion products in seawater and sea-sand concrete. Materials. 2019, 12:3330. 10.3390/ma12203330
48. Wei J, Zhou Y, Dong J, He X, Ke W: Effect of cementite spheroidization on improving corrosion resistance of pearlitic steel under simulated bottom plate environment of cargo oil tank. Materialia. 2019, 6:100316. 10.1016/j.mtla.2019.100316
49. Shi L, Song Y, Dong K, Wang H, Shan D, Han EH: The change of cathode/anode roles and corrosion forms in 2024/Q235/304 tri-metallic couple with the variation of oxygen concentrations and area ratios. Corrosion Science. 2021, 184:109400. 10.1016/j.corsci.2021.109400
50. Tian Y, Liu Y, Xie YM, et al.: Coupled effects of chlorides and sulfates on steel reinforcement corrosion in concrete structures: A comprehensive review. Case Studies in Construction Materials. 2025, 22:e04263. 10.1016/j.cscm.2025.e04263
51. da Fonsêca MSDAB, Meira GR: Accelerated chloride-induced corrosion of hot-dipped galvanized reinforcements and its influence on bond strength to concrete. Construction and Building Materials. 2024, 426:136123. 10.1016/j.conbuildmat.2024.136123
52. Valdez B, Ramirez J, Eliezer A, Schorr M, Ramos R, Salinas R: Corrosion assessment of infrastructure assets in coastal seas. Journal of Marine Engineering & Technology. 2016, 15:124-34. 10.1080/20464177.2016.1247635